Astron. Astrophys. 356, 327–334 (2000)

ASTRONOMY AND ASTROPHYSICS

Remote diagnostic of the heliospheric termination shock using neutralized post shock pick-up ions as messengers

H.J. Fahr and G. Lay

Institut für Astrophysik und Extraterrestrische Forschung, Universität Bonn, Auf dem Hügel 71, 53121 Bonn, Germany

Received 11 June 1999 / Accepted 26 January 2000

Abstract. Hydrogen pick-up ions when produced in the inner heliosphere are convected outwards with the solar wind and are accelerated by nonlinear wave-particle interactions. Upon their arrival at the solar wind termination shock the highest percentage of them passes over from the preshock to the postshock plasma regime. At this occasion these ions suffer a characteristic change in their density and velocity distribution which sensitively reflects the shock properties. We calculate the postshock pick-up ion spectrum and demonstrate the influence of the density compression factor realized at the shock. We then calculate the distribution function of keV–Energetic Neutral H-Atoms (H-ENAs) originating as products of these postshock pick-up ions decharged by local H–atoms and show how, by detection of spectral H-ENA fluxes at the earth's orbit, a very efficient remote diagnostic of the shock properties, especially the shock compression ratio, is enabled. ENAs up to energies of 5 keV clearly reflect the preshock plasma conditions, those at energies larger than 10 keV the postshock plasma conditions. In the energy range between 5 through 50 keV decharged H^+ pick-up ions strongly dominate over all competing ENA fluxes which were discussed in the literature up to now.

Key words: solar system: general – inteplanetary medium

1. Introductory remarks

Since decades now the location and geometry of the solar wind termination shock has been a subject of intensive theoretical investigations (for a thorough recent review see Zank 1999), though up to now no shock structure could yet be identified by the deep-space NASA spaceprobes, neither by direct nor indirect signatures. Meanwhile not only the location but even more the structure of this shock has become an object of prime interest since the multi-fluid character of this shock transition has clearly been recognized (Donohue & Zank 1993; Zank et al. 1993; Chalov & Fahr 1994, 1995, 1997; LeRoux & Fichtner 1997; Kausch & Fahr 1997; Fahr et al. 2000). Dependent on the degree of the cosmic-ray-induced shock modulation and the pick-up ion injection efficiency at the shock for instance density compression ratios between 1 through 6.5 can be expected. Furthermore not only will the shock be a non-classical one (i.e. classical Rankine-Hugoniot relations may not be applicable), it is also pointed out to be a weak shock with preshock solar wind Mach numbers much smaller than expected earlier (see Fahr & Rucinski 1999).

Since many open problems are outstanding in this field, any form of a new shock diagnostic will be highly appreciated by the science community. With concern to this fact already in the recent past energetic neutral atom (ENA) imaging has been proposed in the literature for the remote study of planets, comets and of outer heliospheric plasma structures (see Roelof 1987, 1992; Gruntman 1992, 1997; Hsieh et al. 1991, 1992; Hsieh & Gruntman 1993; Williams et al. 1992; Barabash et al. 1995; Dubinin & Lundin 1995; Czechowski & Grzędzielski 1998; Scime et al. 1994; Funsten et al. 1994).

Concerning the distant heliospheric plasma scenarios one may easily realize that all dechargeable plasma species in subsonic flow with respect to the solar restframe produce specific ENA's which can be detected at the earth's orbit. First Gruntman (1992) had calculated that shocked solar wind protons from regions downstream of the termination shock upon charge exchange with neutral H-atoms produce low energetic H-ENA's and at energies larger than 0.4 keV yield total fluxes of about 30 [$cm^{-2}s^{-1}$ $ster^{-1}$] at the earth's orbit. In addition Hsieh et al. (1991, 1992) had pointed out that also H-ENA's with energies larger than 1 keV can be expected from regions beyond the termination shock due to charge exchange reactions of anomalous cosmic ray H-particles (H-ACR's) with interstellar neutral H-atoms. As they could show spectral fluxes of between 10^{-3} and 10^{-11} [$cm^{-2}s^{-1}ster^{-1}keV^{-1}$] are to be expected at the earth in the energy range between 1 and 100 keV.

Also the EUV resonance glow emission backscattered from postshock O^+ pick-up ions was proposed to be profitably usable as an appropriate tracer to the postshock plasma conditions (Gruntman & Fahr 1998, 1999), as long as their resonance glow can be disentangled from that of the interstellar O^+ ions beyond the heliopause. But different from all these earlier proposals for remote sensing of the regions downstream of the solar wind shock, as we shall show in the following sections of this paper, keV-energetic H-atoms originating in the postshock region

Send offprint requests to: Hans J. Fahr
Correspondence to: (hfahr@astro.uni-bonn.de)

from local pick-up ion dechargings by H-atoms and detected by ENA detectors at 1 AU are probably the most suitable, and in fact the only available candidates to communicate clearly to us the actual shock properties and the resulting postshock thermodynamic plasma conditions. As we are going to prove in this paper this is due to the fact that postshock pick-up ENA's represent the dominant contribution to H-ENA fluxes in the range from 10 to 100 keV and that the spectral profile of these fluxes in this range gives the only available, observational hint to the actual compression ratio at the shock. This compression ratio by itself reflects the degree of modulation of this shock by energetic particles like ACR's (e.g. see Chalov & Fahr 1997).

2. Calculation of pick-up ion ENA spectra

The pitch-angle isotropized distribution function of pick-up ions, $f(t, \boldsymbol{r}, v)$, is found as the solution of the following kinetic transport equation (see e.g. Lee 1983; Isenberg 1987; Bogdan et al. 1991):

$$\frac{\partial f}{\partial t} + \boldsymbol{U}\frac{\partial f}{\partial \boldsymbol{r}} = \frac{1}{v^2}\frac{\partial}{\partial v}\left(v^2 D \frac{\partial f}{\partial v}\right) + \frac{v}{3}\frac{\partial f}{\partial v}\mathrm{div}(\boldsymbol{U}) + S(\boldsymbol{r}, v). \quad (1)$$

where $\boldsymbol{U}(\boldsymbol{r})$ is the solar wind velocity, v is the velocity of pick-up ions in the solar wind rest frame, $D(\boldsymbol{r}, v)$ is the energy diffusion coefficient for pick-up ions, and $S(\boldsymbol{r}, v)$ is the local production rate of freshly ionized particles.

Chalov et al. (1995, 1997) have used a spherical coordinate system (r, ϑ, φ) with the Sun as its origin and the polar axis pointed in the interstellar upwind direction (i.e. $\vartheta = 0$ = LISM upwind direction) and have solved the above transport equation after introduction of the differential phase space density, $N = 2\pi r^2 \sin(\vartheta) v^2 f$, in the following equivalent form:

$$\frac{\partial N}{\partial t} = -\frac{\partial}{\partial r}(uN) - \frac{\partial}{\partial \vartheta}\left(\frac{w}{r}N\right) - \quad (2)$$
$$-\frac{\partial}{\partial v}\left[\left(\frac{\partial D}{\partial v} + \frac{2D}{v} - \frac{v}{3r^2}\frac{\partial u r^2}{\partial r} - \frac{v}{3r\sin\vartheta}\frac{\partial w \sin\vartheta}{\partial \vartheta}\right)N\right] +$$
$$+\frac{1}{2}\frac{\partial^2}{\partial v^2}(2DN) + 2\pi r^2 \sin\vartheta\, v^2 S(r, \vartheta),$$

where $u = u(r, \vartheta)$ and $w = w(r, \vartheta)$ are the radial and tangential components of the mass-loaded solar wind velocity. Eq. (2) is then solved numerically by further converting this nonlinear partial differential equation of second order into an equivalent system of linear stochastic differential equations (SDE-system!). For further details see Chalov et al. (1995, 1997).

Neutral LISM H atoms penetrate the interface region between the solar wind and the interstellar plasma and eventually appear in the inner heliosphere being subject to ionization processes there. Where and when these neutral atoms are ionized, they there and then contribute to a specific H^+ pick-up ion production rate. The local heliospheric pick-up H^+-production rates are thus given by the following formula (for details see Rucinski et al. 1993):

$$q(\boldsymbol{r}) = n_{\mathrm{H}}(\boldsymbol{r})[\nu_{\mathrm{ph}}(\boldsymbol{r}) + \nu_{\mathrm{ex}}(\boldsymbol{r})], \quad (3)$$

where $n_{\mathrm{H}}(\boldsymbol{r})$ is the number density of the neutral H-atoms in the heliosphere, and $\nu_{\mathrm{ph}}(\boldsymbol{r})$ and $\nu_{\mathrm{ex}}(\boldsymbol{r})$ are the relevant local photoionization and charge exchange frequencies. In the papers by Chalov et al. (1995, 1997) the densities $n_{\mathrm{H}}(\boldsymbol{r})$ both for the pre- and the postshock regions are calculated within the self-consistent twin-shock interface model developed by Baranov & Malama (1993). The total pick-up ion production rate given by Eq. (3) is then simply related to the source $S(r, \vartheta)$ in Eq. (2) by

$$q(r, \vartheta) = 4\pi \int v^2 S(r, \vartheta) dv. \quad (4)$$

At their production pick up ion velocities seen from the solar wind rest frame are assumed to be identical with the local solar wind velocity $\boldsymbol{u}$, i.e. the source function hence attains the form: $S \propto \delta(\boldsymbol{v} - \boldsymbol{u})$.

The pick-up ion spectra are obtained as numerical integrations of the above mentioned SDE-system of linear differential equations on the basis of a sample of 500000 probability carriers (test particles). The resulting spectra as function of distance and velocity reflect the effects of convection, adiabatic cooling, and momentum diffusion. For the purpose of the following calculations of pick-up ENA spectra resulting from charge-exchange reactions of pick-up ions with local H-atoms we will not start out again from the time-consuming SDE calculations, but instead we first aim here at an appropriate fit of the already obtained spectra.

3. Fit procedure applied to the SDE calculations

3.1. Fit of the preshock pick-up ion data

The SDE-calculations by Chalov et al. (1995) which were briefly explained in the section above deliver differential particle fluxes $\Phi^{\mathrm{pui}} = [4\pi f^{\mathrm{pui}}(r, \vartheta, v)u]$ with the dimension: particles/cm^2/s/keV. These fluxes are connected with the usual distribution function $f^{\mathrm{pui}}(r, \vartheta, v)$ in the solar wind reference frame by:

$$f^{\mathrm{pui}}(r, \vartheta, w) = \frac{1}{4\pi u_0}\Phi^{\mathrm{pui}}(r, \vartheta, w), \quad (5)$$

where the new variable w denotes the normalized particle kinetic energy given by $w = (v/u_0)^2$ with $u_0 = 450$ km/s being the adopted value for the solar wind reference velocity at 1 AU and yielding $(m_{\mathrm{p}} u_0^2/2) \cong 1$ keV.

In view of the extended calculations which are necessary to convert the numerically generated pick-up ion spectra into pick-up ion ENA spectra, we are primarily aiming at in this paper, we first look for an acceptable algebraic representation. We try to represent the pick-up ion spectra by an algebraic algorithm as convenient as possible fitting satisfactorily accurate the numerical results of the above described pick-up ion spectra.

Restricting our interests here to the upwind direction (i.e. $\vartheta \cong 0$) and normalizing radial distances R with R_{E} = 1 AU (in our calculations we are based on a termination shock location at $R_{\mathrm{S}} = 89.7$ AU) by introduction of $X = (R/R_{\mathrm{E}})$ the preshock pick-up ion (PUI) spectra in the range of $1 \leq X \leq X_{\mathrm{S}} = 89.7$

(shown in Fig. 3 of Chalov et al. 1995) are best-fitted by:

$$f_1^{\rm pui}(X,w) = \frac{1}{4\pi}\frac{1}{u_0}\left[C_\gamma(X) w^\gamma \exp\left(-C_\kappa(X)(w-w_0)^\kappa\right)\right]. \quad (6)$$

Here the subscript "1" denotes the preshock spectrum.

Hence the preshock pick-up ion (PUI) spectrum exactly at the position of the shock (i.e. at $X_{\rm S} = 89.7$) is given by:

$$f_1^{\rm pui}(X_{\rm S},w) = \frac{1}{4\pi}\frac{1}{u_0}\left[C_\gamma(X_{\rm S}) w^\gamma \exp\left(-C_\kappa(X_{\rm S})(w-w_0)^\kappa\right)\right]. \quad (7)$$

For normal turbulence levels (i.e. the standard case in Chalov et al. (1995): i.e a turbulence power spectrum with spectral power index $\alpha = -3$; i.e. dissipationless wave propagation!) the following best-fitting set of parameters is obtained:

$$\begin{array}{l} C_\gamma(X) = 10^{4.3141} X^{-0.3363} [{\rm cm}^{-2}{\rm s}^{-1}{\rm keV}^{-1}]; \\ C_\kappa(X) = 0.442\ X^{0.202}; \gamma = -0.1145; \kappa = \frac{2}{3}; \\ w_0 = 0.8330. \end{array} \quad (8)$$

For enhanced turbulence levels including wave generation in interplanetary space one can in a similar way model the case $\alpha = -2$, instead of $\alpha = -3$. This case is also shown in Fig. 3 of Chalov et al. (1995) and in this latter case a fit with the following parameters is found:

$$\begin{array}{l} C_\gamma(X) = 10^{4.1613} X^{-1.2567} [cm^{-2}s^{-1}{\rm keV}^{-1}]; \\ C_\kappa(X) = 0.469\ X^{-0.5741}; \gamma = -0.036; \kappa = \frac{2}{3}; \\ w_0 = 9.7707. \end{array} \quad (9)$$

The spectra obtained on the basis of the above fit representations are shown in Fig. 1 for different solar upwind distances $R_{\rm i} = X_{\rm i} R_{\rm E}$ with:

$$X_1 = 15; X_2 = 35; X_3 = X_S = 89.7 \quad (10)$$

As one can see, for normal Alfvénic turbulence levels (case A) the spectral intensity of the curves systematically decreases with distance at all energies, even though Fermi-2 acceleration processes counteract adiabatic deceleration processes. This is different for the spectral intensity curves resulting for enhanced turbulence levels (case B), since here Fermi-2 acceleration processes are overcompensating adiabatic deceleration processes at energies larger than 100 keV.

3.2. Fit of the postshock pick-up ion data

In the next step we are interested in the changes of the pick-up ion spectrum resulting downstream of the shock, i.e. after the pick-up ions arriving at $X = X_{\rm s}$ with a spectrum given by Eq. (7) have passed over the shock, except for those undergoing a reflection at the potential ramp of the shock and moving upstream again. The relative abundance of the latter is calculated by Chalov & Fahr (1996) to be of the order or less than 5 percent for quasi perpendicular shocks. In our following notation we shall use an index "1" for upstream quantities and an index "2" for corresponding downstream quantities. When passing over the shock the following changes in the PUI distribution function have to be considered:

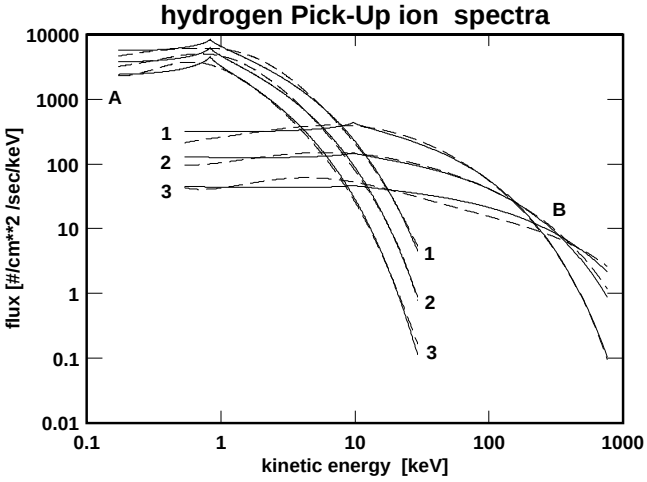

Fig. 1. Shown are calculated (dashed) and fitted (full) spectra of H^+ pick-up ions as function of energy in keV for various distances: 1: R = 15 AU; 2: R = 35 AU; 3: R= 89 AU. Curves A are for normal turbulence levels, curves B for enhanced turbulence levels.

a) total densities are increased by the compression ratio: $s = u_1/u_2 = \rho_2/\rho_1$,
b) due to an increase in the magnetic field magnitude by the factor s (i.e. normal shock condition as expected for $\vartheta \cong 0$: $\boldsymbol{B}\times\boldsymbol{U} = BU$), and due to the conservation of the magnetic moment of pick-ups passing over the shock there is a jump in the energy characterized by: $v_{\perp 2}^2 = s v_{\perp 1}^2$, which for an isotropic distribution $f^{\rm pui}$ implies that: $\langle v_\perp^2 \rangle = (2/3)v^2$. This thus gives the result: $v_2^2 = s v_1^2$,
c) due to the differential phase space flow conservation over the shock (i.e. Liouville theorem) one obtains:

$$f_1^{\rm pui}(X_{\rm S},v_1) d^3v_1 u_1 = f_2^{\rm pui}(X_{\rm S},v_2) d^3v_2 u_2 \quad (11)$$

which leads to:

$$\begin{aligned} f_2^{\rm pui}(X_{\rm S},v) &= f_1^{\rm pui}(X_{\rm S},v_1(v)) \frac{u_1}{u_2}\frac{d^3v_1}{d^3v_2} \\ &= s J(v_1,v_2) f_1^{\rm pui}(X_{\rm S},v_1(v)), \end{aligned} \quad (12)$$

where $J(v_1,v_2)$ is the Jacobian of the transformation of preshock to postshock velocities given by: $J(v_1,v_2) = (4\pi v_1^2 dv_1/4\pi v_2^2 dv_2) = s^{-(3/2)}$.

When taking all these changes together this then leads to the following result:

$$f_2^{\rm pui}(X_{\rm s},w) = s^{-\frac{1}{2}} f_1^{\rm pui}(X_{\rm s}, s^{-1}w). \quad (13)$$

In view of Eq. (6) this then leads to the following postshock PUI spectrum:

$$\begin{aligned} f_2^{\rm pui}(X_{\rm S},w) &= s^{-\frac{1}{2}}\frac{1}{4\pi}\frac{1}{u_0}\left[C_\gamma(X_{\rm S}) s^{-\gamma} w^\gamma \right. \\ &\quad \left. \exp\left(-C_\kappa(X_{\rm S}) s^{-\kappa}(w-w_0)^\kappa\right)\right]. \end{aligned} \quad (14)$$

The postshock pick-up ion spectrum developed in the form of the above Eq. (14) is shown in Fig. 2 for cases A and B and

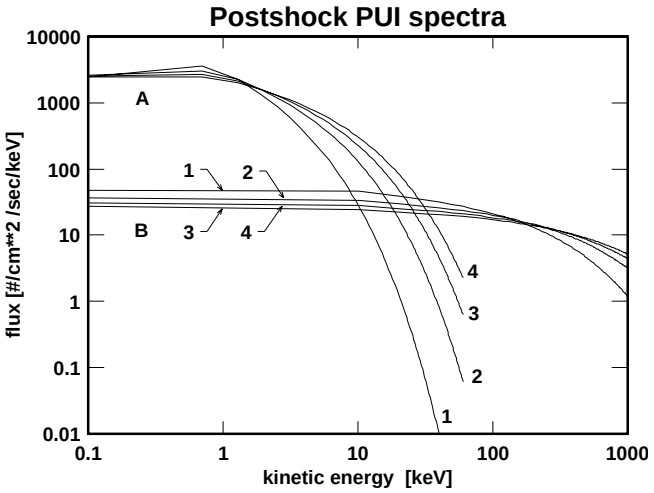

Fig. 2. Shown are spectra of H^+ pick-up ions in the postshock region (i.e. $X \geq X_S$) as function of energy in keV for various compression ratios s = 1,2,3,4. The postshock spectra are derived with the help of the preshock spectra at $X = X_S$ (see Fig. 1). Curves A are for normal turbulence levels, curves B for enhanced turbulence levels.

various compression ratios s at the termination shock, i.e. at $X_S = 89.7$. The case $s = 4$ characterizes the strong classical shock, whereas cases $s \leq 4$ characterize particle-modulated shocks (see Chalov & Fahr 1997). For $s = 1$ no shock compression is realized, i.e. a shockfree deceleration down to subsonic velocities occurs, and thus pre- and postshock pick-up ion spectra at $X_S = 89.7$ are identical. For increasing compression ratios $s \geq 1$ the shock is becoming harder and as a consequence, as seen in Fig. 2, the spectral intensities are increased in the range between 1 to 100 keV. In the energy range between 20 to 100 keV the spectral intensity is highly sensitive with respect to s increasing by more than 3 orders of magnitude between cases: $s = 1$ and $s = 4$. Though for higher turbulence levels (case B) the spectral intensities in these energy ranges in comparison are even higher, on the other hand they are less sensitive to the compression ratio s. At normal turbulence levels (case A) it is, however, obvious that the spectral intensity slope in the range between 10 to 100 keV clearly reflects the compression ratio s, and/or the other way around the actually prevailing turbulence level in the inner heliosphere.

Starting with the above formulated pick-up ion spectrum given by Eq. (14) one could again proceed with the aforementioned SDE calculations (Chalov et al. 1995, 1997) in the postshock region, now evaluating all quantities relevant within the particle transport equation, i.e. Eq. (2), for the postshock plasma conditions as presented in the twin-shock model by Baranov & Malama (1993). Together with the actually prevailing postshock diffusion coefficients and the flux geometry valid along the upwind axis, one could derive local pick-up ion spectra in the postshock region and could then use these spectra to calculate postshock pick-up ion ENAs. This ambitious work we plan to do in a forthcoming paper (Chalov & Fahr 2000). Here in view of the extended computational efforts which were necessary within the above mentioned procedure we shall, however, prefer to use an approximative, but very reasonable approach allowing both a highly informative and straightforward calculation of postshock pick-up ENA spectra along the following line of argumentation:

Starting from the general transport equation given by Eq. (1) and looking now for its solutions in the region downstream of the termination shock one finds:

$$\boldsymbol{U}_2 \frac{\partial f}{\partial \boldsymbol{r}} = \frac{1}{v^2}\frac{\partial}{\partial v}\left(v^2 D_2 \frac{\partial f}{\partial v}\right) + \frac{v}{3}\frac{\partial f}{\partial v}\mathrm{div}(\boldsymbol{U}_2) - L_2(\boldsymbol{r}, v). \quad (15)$$

where $\boldsymbol{U}_2$ is the downstream solar wind bulk velocity, D_2 is the momentum diffusion coefficient in this region, and $\boldsymbol{L}_2(\boldsymbol{r}, v)$ denotes charge-exchange-induced losses of postshock pick-up ions. The corresponding charge-exchange-induced gains are practically absent, since the H-atom distribution function even when seen from the wind frame does not contain energies in the PUI-relevant 10 - to 100 KeV range.

The postshock solar wind plasma represents a low Mach-number flow. Thus one can well assume that at such posthock Mach numbers of below $M_2 \leq 0.2$ the plasma flow behaves nearly incompressible as explicitly proven by Fahr et al. (1993) or Scherer et al. (1994). Thus the mass flow continuity requirement for solar wind protons simply states that: $\mathrm{div}(\rho \boldsymbol{U}_2) = \rho_2 \mathrm{div}(\boldsymbol{U}_2) = 0$. As a consequence the pick-up ion adiabatic deceleration term (second term on the LHS of Eq. (15)) connected with $\mathrm{div}(\boldsymbol{U}_2)$ vanishes.

The first term on the LHS of Eq. (15) describes the Fermi-2 acceleration term due to wave-particle interactions. The governing momentum diffusion coefficient $D_2(\boldsymbol{r}, v)$ as used in Chalov et al. (1995) was derived in its general form by Schlickeiser (1989) and it is shown to depend essentially, apart from the particle velocity, on the local Alfvénic turbulence levels, the turbulence cross helicity, the Alfvén speed and the spectral index of the turbulence spectrum. All of these quantities are not well predictable for the downstream region. As it seems to us, there is, however, the following good argument why Fermi-2 acceleration may be considered as unimportant in the downstream region, at least in many cases depending on the angle between the local shock normal and upstream solar wind flow vector.

One can assume that the termination shock is probably the only active Alfvén wave generator for the downstream region. Turbulences are convected to this shock from upstream, but for moderate upstream Alfvénic Mach numbers with $M_{A1} \leq \sqrt{s}$ only those waves with phase velocities parallel to $\boldsymbol{B}$ can propagate from there into the downstream region, whereas those with phase velocities antiparallel cannot, but are sticking at the shock. The shock thus may operate as a cross-helicity converter, converting the cross-helicity $h_{c1} = 0$ of the upstream turbulence into the cross helicity $h_{c2} = 1$ of the downstream turbulence. Connected with $h_c = (1-\epsilon)/(1+\epsilon)$ is the degree of turbulence anisotropy: $\epsilon = I_{0-}/I_{0+}$. In the downstream region we thus under the above mentioned conditions assume that $\epsilon_2 = 0$, since no antiparallel Alfvén waves are expected in this region, i.e. $I_{0-} = 0$ as is also the case in regions close to the corona. The Fermi-2 process, however, only operates when particles can

interact with countermoving waves, since they can only gain energies when they are scattered between upgoing and downgoing wave systems. Since under the above mentioned conditions there are only waves propagating downstream from the shock (i.e. $\epsilon = 0$) this process will not act in the downstream region.

For cases with $M_{\rm A1} \geq \sqrt{s}$ the argumentation may not be as clear as given above. But a consideration of the wave power flux conservation at the shock based on results given by McKenzie & Westphal (1969) shows that for quasi-perpendicular shocks and with $\boldsymbol{B}_1$ being nearly perpendicular to $\boldsymbol{U}_1$ one obtains that $\epsilon_2 \simeq \epsilon_1 \simeq 1$. Though under these conditions antiparallel waves in principle are possible, they may nevertheless be quickly dying out with increasing downstream distances from the shock. In addition it turns out that even for $\epsilon_2 \simeq 1$ the velocity diffusion term in Eq. (15) may be irrelevant in view of the reduced magnitude of diffusion coefficient $D_2(R_{\rm s}, v)$ downstream compared to that $D_1(R_{\rm s}, v)$ upstream. For that argument one can study the ratio $\delta_{2/1} = D_2(R_{\rm s}, v)/D_1(R_{\rm s}, v)$ given by (see Chalov et al. 1995):

$$\delta_{2/1} = \left(\frac{U_2}{U_1}\right)^{\gamma} \left(\frac{v_{\rm A2}}{v_{\rm A1}}\right)^2 \frac{\langle \delta B_2^2 \rangle \, B_1^2}{\langle \delta B_1^2 \rangle \, B_2^2} \tag{16}$$

where $\gamma = 5/3$ is the spectral power index of the upstream turbulence spectrum, and where $\langle \delta B_1^2 \rangle$ and $\langle \delta B_2^2 \rangle$ are the normalized, upstream and downstream wave power amplitudes. If this expression is evaluated for the conditions at a perpendicular shock with $\boldsymbol{B}_1$ nearly perpendicular to $\boldsymbol{U}_1$ one then obtains the result:

$$\delta_{2/1} = \left(\frac{1}{s}\right)^{\gamma} s \frac{1+s}{2s} \tag{17}$$

If this expression is evaluated for a high Mach number shock with $s = 4$ one then obtains: $\delta_{2/1} \simeq 0.24$, meaning that the velocity-diffusion term (first term on the LHS of Eq. (15)!) even at $\epsilon_2 \simeq 1$ is of inferior importance compared to its relevance in the upstream region. We thus omit this term in the downstream transport equation (15) and are left with:

$$\boldsymbol{U}_2 \frac{\partial f}{\partial \boldsymbol{r}} = -L_2(\boldsymbol{r}, v) = -\beta_2(r, v) f. \tag{18}$$

With the charge exchange cross section $\sigma(v_{\rm rel})$ given by Eq. (22) we can then simply obtain from Eq. (18) the result:

$$f(r, v) = f_2^{\rm pui}(X_{\rm S}, v) \exp\left(-\beta_2(v) \int\limits_{R_{\rm S}}^{r} \frac{dr'}{U_2(r')}\right) \tag{19}$$

where $f_2^{\rm pui}(X_{\rm s}, v)$ is the postshock pick-up ion spectrum, and where β_2 is equal to: $\beta_2 = n_{\rm H} n_2^{\rm pui} \langle \sigma(v) v_{\rm rel}(v) \rangle$. Recalling then that the argument of the exponential function generally is shown to be of the order of 10^{-2} or smaller will then reveal that Eq. (17) can reasonably well be approximated by:

$$f(r, v) = f_2^{\rm pui}(X_{\rm S}, v). \tag{20}$$

Thus we can well assume that the pick-up ion spectrum is not substantially changing in shape with increasing distance from the shock in downstream direction. We may then be justified to assume a nearly invariable pick-up ion spectrum along the stagnation line up to the heliopause which according to Baranov & Malama (1993) is adopted at $R_{\rm H} = 150$ AU = 1.67 $R_{\rm S}$. With this idea we then arrive at the following calculation of pick-up ENA spectra:

4. Conversion of pick-up protons into H-ENAs

Pick-up protons with a specific rate are locally subject to resonant charge exchange processes with interstellar H-atoms resulting in H-ENA fluxes which can be well observed inside the inner heliosphere.

Looking with an appropriate ENA detector from a position at the earth's orbit along a radial line of sight, with a solid angle of view $d\Omega = 2\pi[1 - \cos\vartheta_v]$ coaligned with the stagnation line, one collects ENA particles positioned within the velocity intervall Δv at a velocity v which at some distance R and an increment dR on the line of sight are produced with the following differential rate:

$$dq(X, v) dv dR d\Omega = \tag{21}$$
$$2\pi[1 - \cos\vartheta_v] R_{\rm E} dX \left[f^{\rm pui}(X, v) v_{\rm rel} \sigma_{\rm rel} n_{\rm H}(X) v^2 dv\right]$$

with $v_{\rm rel}$ and $\sigma_{\rm rel} = \sigma(v_{\rm rel})$ being the relative velocity between H-atoms and pick-up ions and $\sigma_{\rm rel}$ as the associated charge exchange cross section given by (Maher & Tinsley 1977):

$$\sigma(v_{\rm rel}) = \left[1.64\ 10^{-7} - 1.6\ 10^{-8} \log(\bar{v}_{\rm rel})\right]^2 {\rm cm}^2 \tag{22}$$

where $\bar{v}_{\rm rel}$ is the relative velocity measured in units of [cm/s].

Keeping in mind that at larger distances (i.e. ≥ 10 AU) H-atoms have an approximately constant heliospheric density of $n_{\rm H} \cong 0.85$ cm^{-3} and a constant bulk velocity of 25 km/s negligible with respect to the pick-up ion velocities v (see Baranov & Malama 1993) we obtain from this rate the differential flux contribution $d\Phi_{\rm ENA}$ by introducing again the associated energy variable $w = v^2/u_0^2$ and we find:

$$d\Phi_{\rm ENA}(X, w)\ dw\ dR\ d\Omega = \tag{23}$$
$$\frac{n_{\rm H}}{2} R_{\rm E} dX\ u_0^4 2\pi(1 - \cos\vartheta_v) \left[\tilde{f}^{\rm pui}(X, w) \sigma_{\rm rel}(w) w\ dw\right]$$

Reminding that in the aforegoing section we have developed the pick-up ion distribution function $f^{\rm pui}$ in the local solar wind rest frame, but want to calculate ENA fluxes in the solar rest frame, we consequently arrive at the following solution:

$$d\Phi_{\rm ENA}(X, w)\ dw\ dR\ d\Omega = \frac{n_{\rm H}}{2} \cdot \tag{24}$$
$$\cdot R_{\rm E} dX\ u_0 2\pi(1 - \cos\vartheta_v) \left[f^{\rm pui}(X, w^w) \sigma_{\rm rel}(w) w^w\ dw^w\right]$$

where w^w is given as the following function of w:

$$w^w = w + 2\sqrt{w} + 1, \tag{25}$$

and where the energy increments dw^w and dw are related by:

$$dw^w = dw(1 + \frac{1}{\sqrt{w}}). \tag{26}$$

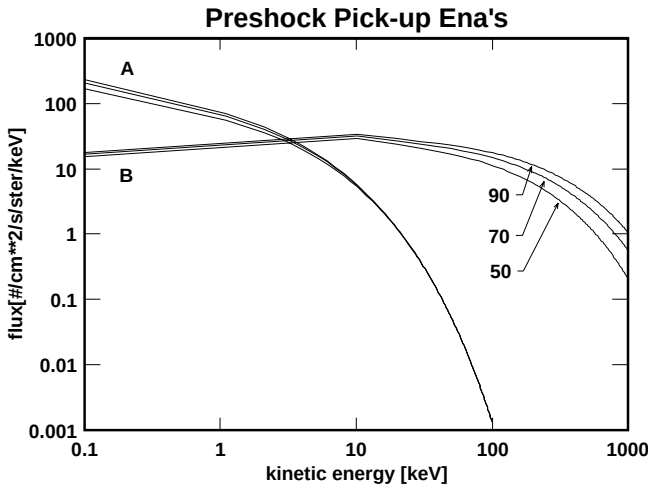

Fig. 3. Shown are preshock pick-up H-ENA spectra as function of energy in keV for various distances of the termination shock, i.e. for $R_{\rm s}$ = 50, 70, 90 AU. Curves A are for normal turbulence levels, curves B for enhanced turbulence levels.

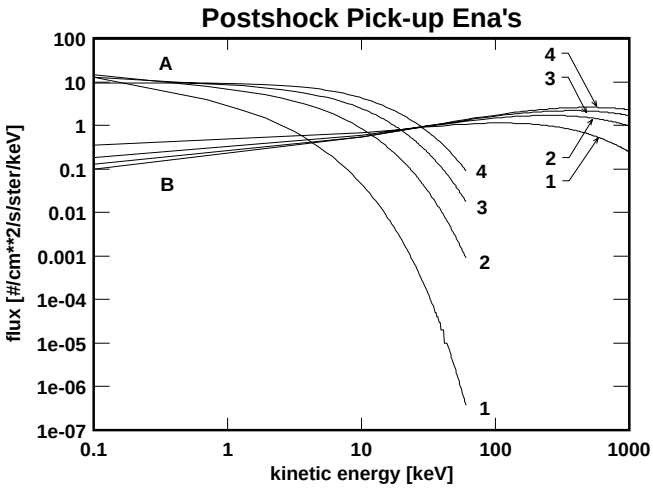

Fig. 4. Shown are postshock pick-up H-ENA spectra as function of energy in keV for various compression ratios s at the shock, i.e. s = 1, 2, 3, 4. Curves A are for normal turbulence levels, curves B for enhanced turbulence levels.

Thus when looking for the integral ENA flux at the earth in units of [cm^{-2}s^{-1}ster^{-1}keV^{-1}] we obtain for the preshock case the following expression:

$$\Phi_{\rm ENA}(X_{\rm E},w) = \frac{n_{\rm H}}{2} R_{\rm E} u_0 \sigma_{\rm rel}(w) \qquad (27)$$
$$\cdot[w+2\sqrt{w}+1][1+\frac{1}{\sqrt{w}}] \int\limits_1^{X_{\rm S}} dX\ f^{\rm pui}(X,w^w)$$

The corresponding ENA fluxes produced by postshock ENA atoms consequently and according to the approximations mentioned at the end of the foregoing section of this paper (i.e. constant spectra in the downstream region) can then be approximated by:

$$\Phi_{\rm ENA}(X_{\rm E},w) = \qquad (28)$$
$$\frac{n_{\rm H}}{2} R_{\rm E} \int\limits_{X_{\rm S}}^{X_{\rm H}} dX u_0 f_2^{\rm pui}(X,w^w)\sigma_{\rm rel}(w) w^w (1+\frac{1}{\sqrt{ws}})$$

with w^w in this postshock case given by:

$$w^w = w + 2\sqrt{\frac{w}{s}} + \frac{1}{s}. \qquad (29)$$

and with $X_{\rm H} = R_{\rm H}/R_{\rm E} = 1.67 X_{\rm S}$ being as mentioned the upwind distance of the heliopause. Eq. (28), assuming invariable postshock PUI spectra along the stagnation line from $X = X_{\rm s}$ (TS shock) up to $X = X_{\rm H}$ (heliopause) as made plausible above, then can be evaluated to yield:

$$\Phi_{\rm ENA}(X_{\rm E},w) = \qquad (30)$$
$$\frac{n_{\rm H}}{2} R_{\rm E} (X_{\rm H}-X_{\rm S}) u_0 f_2^{\rm pui}(X_{\rm S},w^w)\sigma_{\rm rel}(w) w^w (1+\frac{1}{\sqrt{ws}}).$$

In Fig. 3 we have first shown the ENA fluxes resulting from H-atoms arriving from the upwind direction at 1 AU calculated on the basis of Eq. (27) (i.e preshock pick-up ENAs). As we demonstrate fluxes are strongly different for case A and B, respectively, whereas a variation of the shock location using values $X_{\rm S} = 50; 70; 90$ does not imply a sensitive reaction of the spectral fluxes. Fluxes thus are not highly sensitive to the location, but to the compression ratio at the shock.

In contrast, the results in Fig. 4 are based on the postshock pick-up ion dechargings leading to ENA fluxes given by Eq. (30). Here again a strong reaction to the shock compression ratio s can be seen increasing ENA fluxes in the range between 10 to 100 keV by more than 4 orders of magnitude when the shock becomes harder $(s \to 4)$. For higher turbulence levels (case B) this sensitivity with respect to s will only become evident at higher energies between 100 keV to 1 MeV.

5. Conclusions with respect to the diagnostic potential of ENAs

Since transcharged protons of the supersonic preshock solar wind such as as H-ENAs only have velocity vectors pointing out of the solar system, they do not appear in the inner regions of the heliosphere or at 1 AU, unless they have been produced inside the orbit of the earth, i.e. when appearing as transcharged solar wind. Bleszynski et al. (1992), Gruntman (1994) and Bzowski et al. (1996) have calculated H-atom fluxes arriving at the earth (1 AU) due to solar wind protons transcharged by H- and He-atoms inside the orbit of the earth. ENA detectors would detect these fluxes only if they are pointed with their lines of sight to targets very close to the sun, since solar wind ENAs are strongly focussed to a very narrow cone in velocity space. The latter is due the fact that the solar wind is highly supersonic with a bulk velocity in antisolar direction.

Looking, however, outwards from 1 AU into anti-sunward directions an ENA detector thus would not see contributions from transcharged solar wind protons at all, at least not upstream of the termination shock. It thus only collects contributions

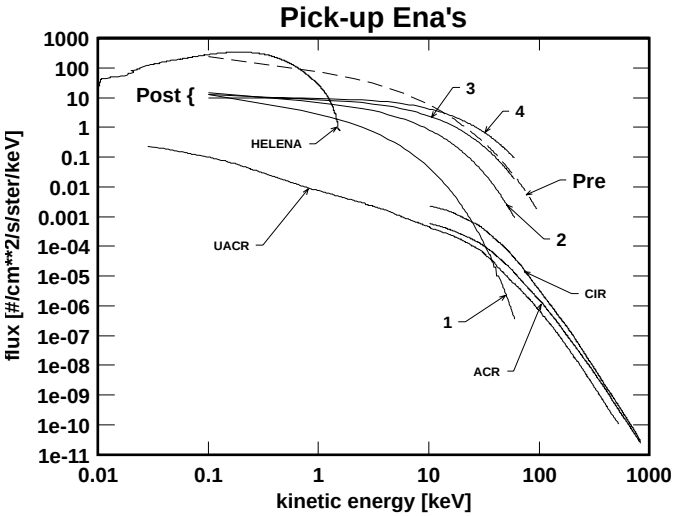

Fig. 5. Pre- and post-shock pick-up H-ENA spectral fluxes are shown as functions of energy in keV units. In all of these curves only the case A: normal turbulence levels, is shown. The postshock spectra are displayed for various compression ratios, i.e. s = 1, 2, 3, 4. Also shown for comparison purposes are competing spectral fluxes of transcharged postshock solar wind protons (Helena's, see Gruntman 1992) of transcharged CIR protons, and of transcharged H-anomalous cosmic rays (CIR and UACR/ACR, see Hsieh et al. 1991, 1992).

from transcharged pick-up ions being subject to charge transfer interactions with H-atoms both inside (upstream) and outside (downstream) of the termination shock. Within the distribution function, as well of preshock as of postshock pick-up ions, one can always identify populated areas with velocity vectors pointing in the sunward direction, i.e. delivering ingoing ENAs after transchargings with H-atoms. Inspection of Figs. 1 and 2 clearly reveal that these calculated, isotropic pick-up ion distributions, valid in the solar wind reference frame, describe large fractions of particles which after decharging produce ENAs going back to the innermost heliospheric regions. In fact all particles with energies larger than 1 keV described by the distribution functions of Figs. 1 and 2 are locally ejected with a geometric probability of $\Delta\Omega/4\pi$ into the sunward direction with a solid angle $\Delta\Omega$. ENA detectors for the registration of keV to MeV neutral H-atoms have been developed, tested and qualified meanwhile by several authors (e.g. see Funsten et al. 1994; Scime et al. 1994).

Thus looking into the upwind direction with a detector placed in an upwind position at 1 AU one would see the resulting ENA fluxes as shown in Figs. 3 and 4. ENA detectors can, however, not discriminate between preshock and postshock ENAs coming in from upwind directions, i.e. they will see the superposition of both ENA types. In Fig. 5 we thus decided to show what a composite ENA spectrum under these conditions could look like. As one may notice there, in the energy range between 0.5 through 2 keV preshock pick-up ion ENA fluxes clearly dominate the spectral intensity, and thus by fitting theoretical results to data obtained in this region one obtains a spectral curve which can safely be extrapolated into the region above 5 keV (see the higher-energy part of the dashed curve in Fig. 5). Data obtained at energies larger than 5 keV then either reveal the dominance or the non-dominance of postshock ENAs. If data are located above the dashed curve then they can clearly be ascribed to postshock ENAs connected with shock compression ratios larger than $s = 2.5$. If, on the other hand, data follow the dashed line, then the contribution of postshock ENAs even in this energy region is inferior and shock compression ratios of $s \leq 2.5$ can be concluded.

Only at energies below 0.5 keV can transcharged postshock solar wind protons (Helenas) be identified which were predicted by Gruntman (1992). The absolute magnitude of spectral ENA fluxes in this low-energy region should, however, also reflect the actual compression ratio at the shock which was not a subject of discussion at the time when Gruntman (1992) wrote his paper. Spectral ENA fluxes from transcharged H-, UACR's/ACR's (Unmodulated/anomalous cosmic ray protons) or from transcharged protons near CIR's (corotating interaction regions) which were predicted by Hsieh et al. (1991, 1992) as evident from Fig. 5 could only be clearly identifiable at energy regions beyond 100 keV.

Acknowledgements. The authors are grateful to the Deutsche Forschungsgemeinschaft for financial support granted within the frame of the scientific projects with numbers *Fa 97/24-1* and *Fa 97/24-2*.

References

Barabash S., Lundin R., Zarnowiecki T., Grzędzielski S., 1995, Adv. Space Res. 16(4), 81
Baranov V.B., Malama Y.G., 1993, JGR 98, 15157
Bleszynski S., Grzędzielski S., Rucinski D., Jakimiec J., 1992, Planet.Space Sci. 40, 1525
Bogdan T.J., Lee M.A., Schneider P., 1991, JGR 96, 161
Bzowski M., Fahr H.J., Rucinski D., 1996, ICARUS 124, 209
Chalov S.V., Fahr H.J., 1994, A&A 288, 973
Chalov S.V., Fahr H.J., 1995, Planet. Space Sci. 43, 1035
Chalov S.V., Fahr H.J., 1996, Solar Phys. 168, 389
Chalov S.V., Fahr H.J., 1997, A&A 326, 860
Chalov S.V., Fahr H.J., 2000, A&A submitted
Chalov S.V., Fahr H.J., Izmodenov V., 1995, A&A 304, 609
Chalov S.V., Fahr H.J., Izmodenov V., 1997, A&A 320, 659
Czechowski A., Grzędzielski S., 1998, Geophys. Res. Letters 25, 1855
Donohue D.J., Zank G.P., 1993, JGR 98, 19005
Dubinin E., Lundin R., 1995, Adv. Space Res. 16(4), 75
Fahr H.J., Rucinski D., 1999, A&A 350, 1071
Fahr H.J., Fichtner H., Scherer K., 1993, A&A 277, 249
Fahr, H.J., Kausch, T., Scherer H., 2000, A&A submitted
Funsten H.O., McComas D.J., Scime E.E., 1994, Optical Engineering 33, 342
Gruntman M.A., 1992, Planet. Space Sci. 40, 439
Gruntman M.A., 1994, JGR 99, 19213
Gruntman M.A., 1997, Rev. Sci. Instruments 65, 758
Gruntman M.A., Fahr H.J., 1998, Geophys.Res.Letters 25(8), 1261
Gruntman M.A., Fahr H.J., 1999, JGR in press
Hsieh K.C., Gruntman M.A., 1993, Adv. Space Res. 13(6), 131
Hsieh K.C., Shih K.L., Jokipii J.R., Gruntman M.A., 1991, In: SOLAR WIND SEVEN, E. Marsch, R. Schwenn (eds.), Pergamon Press, p. 365
Hsieh K.C., Shih K.L., Jokipii J.R., Grzędzielski S., 1992, ApJ 393, 756

Isenberg P.A., 1987, JGR 92, 1067
Kausch T., Fahr H.J., 1997, A&A 325, 828
Lee M.A., JGR 1983, 88, 6109
LeRoux J.A., Fichtner H., 1997, JGR 102, 17365
Maher L.J., Tinsley B.A., 1977, JGR 82, 689
McKenzie J.F., Westphal K.O., 1969, Planet. Space Sci. 17, 1029
Roelof E.C., 1987, Geophys. Res. Lett. 14, 652
Roelof E.C., 1992, in: SOLAR WIND SEVEN, E. Marsch, R. Schwenn (eds.), Pergamon Press, p. 385
Rucinski D., Fahr H.J., S., 1993, Planet. Space Sci. 41, 773
Scherer K., Fahr H.J., Ratkiewicz R., 1994, A&A 287, 219
Schlickeiser R., 1989, ApJ 336, 243
Scime E.E., Funsten H.O., McComas D.J., Moore K.R., Gruntman M.A., 1994, Optical Engineering 33, 357
Williams D.J., Roelof E.C., Mitchell D.G., 1992, Rev. Geophys. Space Phys. 30, 183
Zank G.P., 1999, Space Science Rev. 89, 413
Zank G.P., Webb G.M., Donohue D.J., 1993, ApJ 404, 67